Printed ISSN 1330–0016
Online ISSN 1333–9133
CD ISSN 1333–8390
CODEN FIZBE7

NEW RESULTS ON THE $\mu^+ \to e^+\gamma$ DECAY FROM THE MEG EXPERIMENT

A. PAPA, on behalf of the MEG collaboration

Paul Scherrer Institut, Villigen, Switzerland

Received 4 January 2011; Accepted 9 November 2011
Online 10 January 2012

The aim of the MEG experiment is to measure the branching ratio of the rare muon decay $\mathrm{BR} = \dfrac{\mu^+ \to \mathrm{e}^+\gamma}{\mu^+ \to \mathrm{e}^+\nu_\mathrm{e}\overline{\nu}_\mu}$ at a sensitivity of $\approx 10^{-13}$. To reach this goal, the experiment must use the most intense continuous muon beam available ($\approx 10^8\mu$/s) and obtain the highest energy, time and space resolutions, today reachable. MEG started to collect data at the end of 2008. During 2009 a large part of the data taking time was devoted to calibration measurements and detector performance optimizations; a new physics data sample was collected at the end of this year in 1.5 months of acquisition time. A description of the main features of each subdetector and of the measured resolutions are given and the results of the search for $\mu^+ \to e^+\gamma$ decay based on the 2009 data sample are presented.

PACS numbers: 13.35.Bv, 11.30.Hv, 11.30.Qc, 14.60.Fg UDC 539.126.3
Keywords: lepton flavour violation, MEG experiment, $\mu^+ \to e^+\gamma$

1. Motivation

Lepton flavour violation (LFV) research is presently one of the most promising branches of particle physics for the study of physics beyond the standard model (SM). Flavour violating processes, such as $\mu^+ \to e^+\gamma$, which are not predicted by the minimal standard model (MSM), are very sensitive to the physics beyond it. Neutrino oscillations are now an established fact, which can be accomodated in the SM by including right-handed massive neutrinos and mixing. This modified SM predicts unmeasureable branching ratios (BR) for lepton violating decays. Supersymmetric GUT theories naturally house finite neutrino masses and predict rather large and measurable branching ratios for LFV decays. The $\mu^+ \to e^+\gamma$ process is therefore a powerful tool to investigate physics beyond the SM, since: *a*) the

present experimental upper limit is BR $< 1.2 \cdot 10^{-11}$ at 90% C.L. (by the MEGA collaboration [1]) and *b*) supersymmetric GUT models, such as SO(10) SUSY-GUT or SU(5) SUSY-GUT, predict BR $\approx 10^{-14} - 10^{-11}$ [2–6].

The MEG experiment was designed to reach a sensitivity of BR $\approx 10^{-13}$, two orders of magnitude better than the present experimental limit and within the region of theoretical predictions [7].

Figure 1 shows the previous and the present experimental upper limits on BR($\mu^+ \to e^+\gamma$).

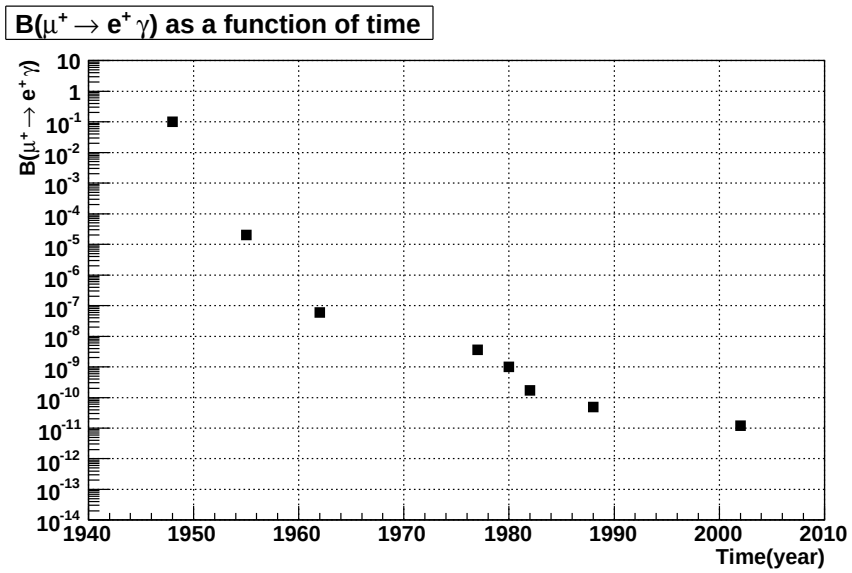

Fig. 1. The previous and the present $\mu \to e\gamma$ branching ratio.

2. The event signature and background

The event signature of the $\mu^+ \to e^+\gamma$ decay at rest is a positron and a photon in timing coincidence, moving collinearly back-to-back with their energies equal to half the muon mass ($m_\mu/2 = 52.8$ MeV). Positive muons are used because they can be stopped in a target without being captured by a nucleus.

Two kinds of background are present: *a*) the correlated background from the radiative muon decay, $\mu^+ \to e^+\nu_e\overline{\nu}_\mu\gamma$, when the positron and the gamma are emitted in opposite directions and the two neutrinos take away a small amount of the total energy and *b*) the uncorrelated background due to an accidental coincidence between a positron from the normal muon decay $\mu^+ \to e^+\nu_e\overline{\nu}_\mu$ and a high energy photon from radiative muon decay or positron annihilation in flight. The latter is the main background source and we evaluated its effective branching ratio at the level of $\leq 10^{-13}$.

3. The experimental set-up

A schematic layout of the MEG detector is shown in Fig. 2. The world's most intense continuous muon beam (available muon intensity $I_\mu = 3\times10^8\mu$/s) is stopped in a thin polyethilene target (thickness $t_{CH_2} = 205\mu$m). The energy, the time and the angle of the gamma are measured by means of the high-energy and time-resolution liquid xenon (LXe) calorimeter; the momentum and the direction of the positron are determined by a very precise spectometer; the positron time is obtained by using the most rapid plastic scintillator detector (the timing counter detector). The detector signals are selected with high efficiency by a trigger system and digitized with high frequency by a data acquisition system (DAQ) based on the DRS chip. All detectors are carefully and frequently calibrated and monitored.

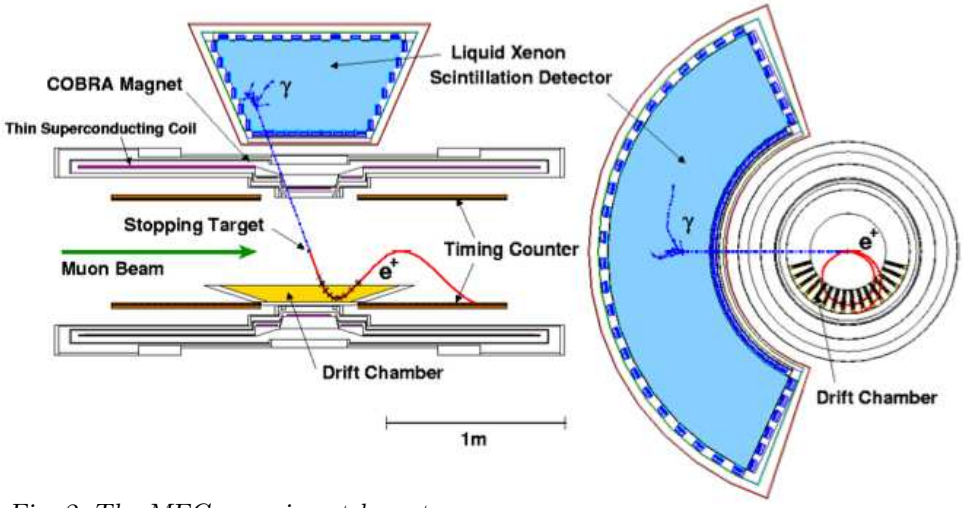

Fig. 2. The MEG experiment layout.

3.1. The muon beam

The muons for MEG are the so-called *surface*-muons [8]. Protons (current 2.2 mA) are accelerated to an energy of 590 MeV by the PSI cyclotron machine and hit a thick graphite target (thickness $t_C = 4$ or 6 mm) where pions are produced. Muons from pions decay at rest emerge from this target. The kinetic energy and the momentum of these surface-muons are ≈ 3.6 MeV and 29 MeV/c respectively. Their range in graphite is ≈ 1 mm; the surface-muons are therefore produced only by π^+-pion decaying close to the target surface.

A pure muon beam at low momentum reaches the thin MEG target for a small straggling and a good identification of the muon decay region. The positron contamination is completly removed by means of the Wien filter and the beam is coupled to the high magnetic field region, where the spectrometer is placed, by the beam transport solenoid (BTS). The last elements of the beam line are shown in Fig. 3.

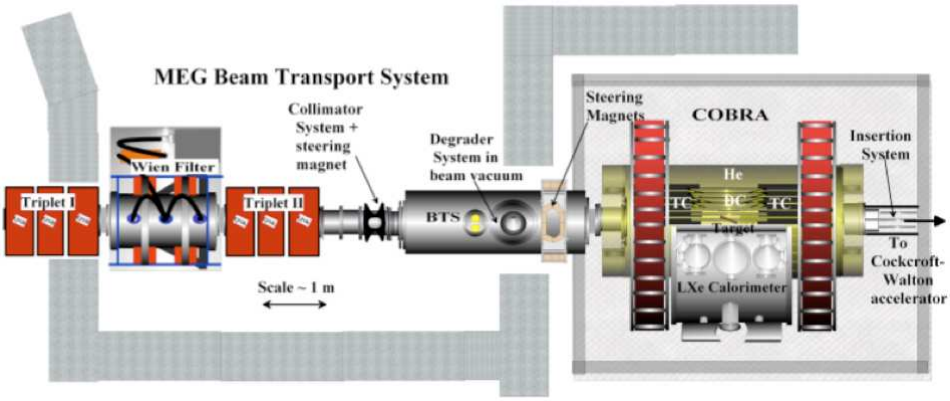

Fig. 3. The elements of the MEG-beam line end.

3.2. The liquid xenon calorimeter

The LXe calorimeter is the larger homogeneous calorimeter using only scintillation light (Fig. 4). The high number of scintillation photons (40000 ph/MeV), the fast time constant (three components $\tau_1 = 4$ ns, $\tau_2 = 22$ ns and $\tau_3 = 45$ ns), the high atomic number (Z = 54), the high density (2.95 g/cm^3) are desirable charac-

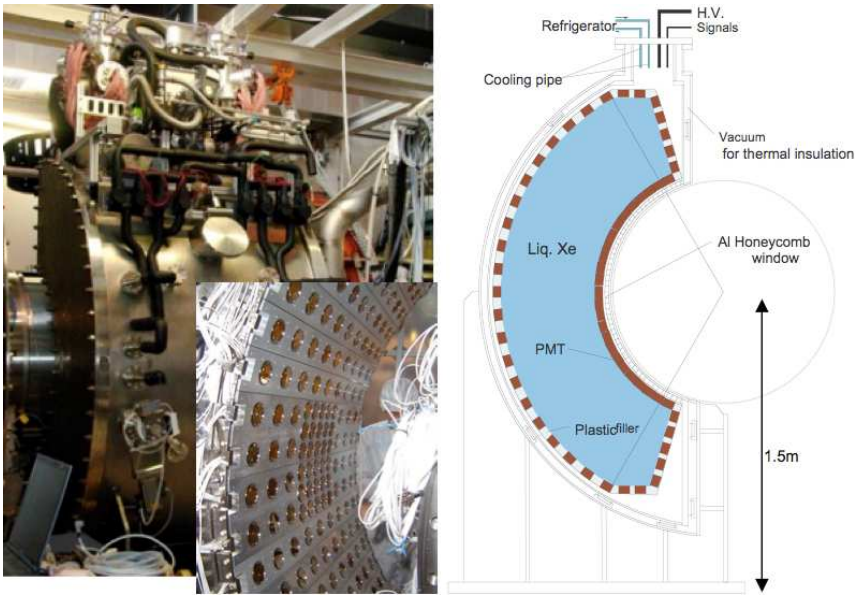

Fig. 4. The liquid xenon calorimeter.

teristics to reach a good energy and time resolutions and to keep the dimensions of the detector relatively small [9]. The detector contains 900 liters of pure liquid xenon. The LXe scintillation light is measured by 846 photomultipliers, immersed in the liquid. A R&D was necessary to ensure that these photomultipliers (Hamamatsu R9869) correctly work at the LXe temperature (≈ -108°C), in the vacuum ultra-violet region (Xenon emission line $\lambda_{\text{scin}} = 178$ nm), at high pulse rate (photomultiplier anodic current ≈ 4 μA) [10].

The γ-energy is directly related to the light intensity measured by the PMTs. The γ is supposed to come from the vertex of a companion positron at the target, and its direction is defined once the γ impact point is determined. The information from all PMTs is used to extract the timing of the γ interaction.

The LXe optical properties, in particular, its transparency strongly affects the performance of this large volume calorimeter. The properties are continuously monitored [11].

Since the calorimeter corresponds to a large volume single vessel, we expect a high rate of low energy γ's. The waveforms of all PMTs are therefore registered to identify the events in which the accidental pile-up of γ-rays occurs.

A study based on a detailed Monte Carlo simulation gives the following predictions: an energy resolution $\Delta E_\gamma/E_\gamma$(FHWM) = 4.5 %, a time resolution Δt_γ(FHWM) ≈ 120 ps and a position resolution Δx(FWHM) = Δy(FWHM) ≈ 1.5 cm.

3.3. The spectometer

The spectometer is made of a drift chamber array mounted inside a high magnetic field region, generated by a superconduting magnet (COBRA magnet).

The main feature of this element is to produce a gradient field along the beam direction, by means of five coils with three different radii: one central, two gradient, and two end coils (Fig. 5). The COBRA nonuniform magnetic field is so shaped as to

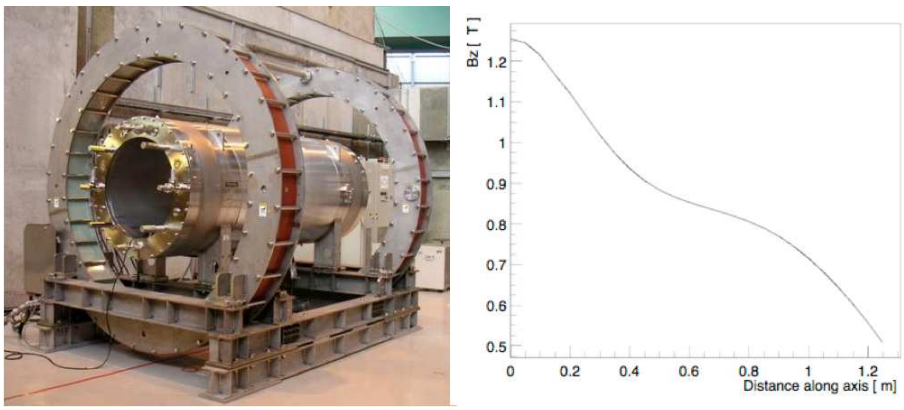

Fig. 5. The superconducting magnet (COBRA magnet) (at left). The magnetic field along the beam direction (at right).

make the projected (in the x-y plane) radius of the positron trajectory depend only on the modulus of the momentum, whatever the positron direction. Low momentum trajectories are confined to a small radius cylindrical region.

Using this field map, the abundant low momentum positrons from muon decays (the Michel's positrons) are swept away from the MEG target, without hitting the chambers and the counters. Rates remain low in the drift chamber system.

Furthermore, positrons emitted at large angles relative to the magnet axis are rapidly removed from the target region in the case of the COBRA nonuniform field. The number of multi-turn trajectories crossing the chambers is minimized and the reconstruction of the higher momentum trajectories is greatly simplified.

The drift chamber array is made of 16 drift chamber sectors radially aligned at 10.5° intervals in azimuth (see Fig. 6). Each sector is made up of two staggered trapezoidal arrays of drift cells. The resolution of the measurements of positron momentum and angle are primarily limited by multiple scattering in the chamber materials and gas. Particular care was paid to reduce this effect. The drift chamber system is filled with a 50% He - 50 % C_2H_6 gas mixture and is surrounded by 100% pure He at 1 atm. Such a choice corresponds to a sufficient ionization loss in the chamber gas (≈ 65 e^-/cm for minimum ionizing particles) and to the minimization of multiple Coulomb scattering effects on trajectories.

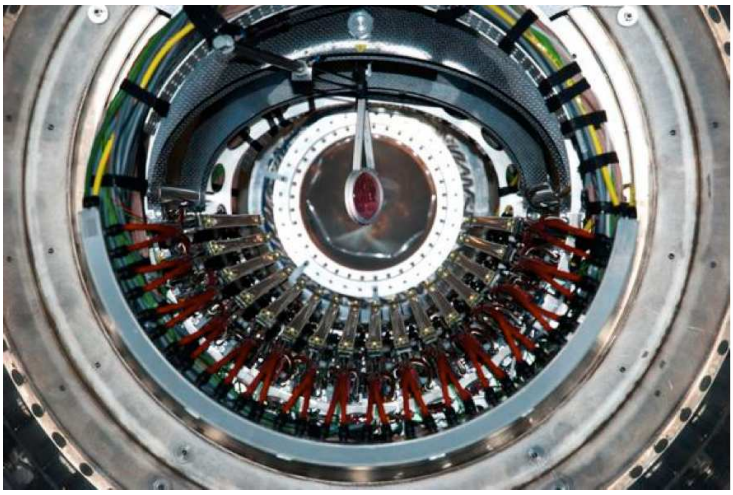

Fig. 6. The drift chambers.

3.4. The timing counter

The timing counter (TC) was designed to measure the positron timing with a resolution of 100 ps (FWHM) (Fig. 7). This fast detector is used, at the trigger level, for selecting events in which a positron is coincident in time and collinear in direction, with a γ detected in the electromagnetic calorimeter.

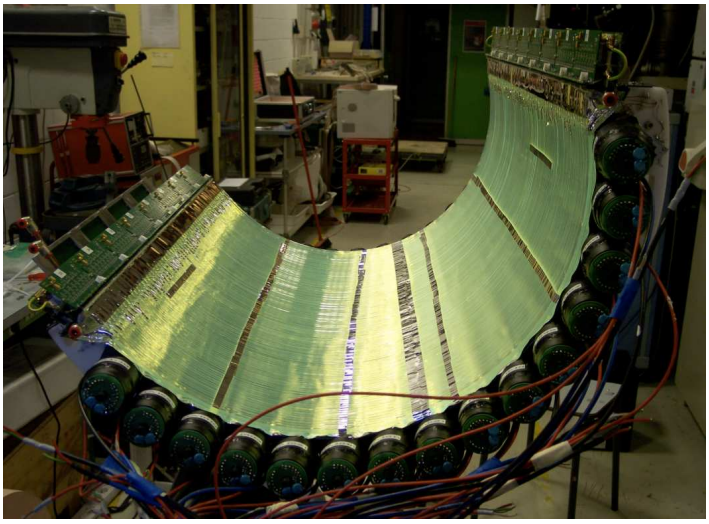

Fig. 7. The timing counter detector.

Two plastic scintillator hodoscopes, half cylinders coaxial with COBRA (made up of 15 scintillator bars) are placed on both sides of the positron spectrometer to detect positrons and provide timing and trigger signals. Each timing counter scintillator bar (BC404 plastic scintillator, $40 \times 40 \times 780$ mm^3) is equipped with two Hamamtsu 2" fine mesh R5924 PMTs. This PMT type can properly operate at high magnetic field (B $\approx$ 1.5 T) [12]. The PMT axis is not aligned with the field, but has a slant angle of 11° corresponding to an optimized performance. The layer of the z-oriented scintillator bars provides an accurate timing of the positron hit, as well as a rough, but fast determination of the corresponding ϕ. The z-coordinate is measured by using the transverse detector. This is made up of two layers of 128 scintillating fibers (BCF20) with square cross-section (5×5 mm^2), equipped at both ends with avalanche photo diodes (APDs) practically insensitive to the magnetic field.

3.5. The trigger system

The trigger system uses the signals coming from the fast detectors (liquid xenon calorimeter and timing counter) to select, with the great efficiency, the $\mu^+ \to e^+\gamma$ candidate events, and effectively rejects background (Fig. 8).

The hardware of the trigger system is based on two different electronics boards.

The first board (Type 1, with 16 FADCs and 1 FPGA) receives the analog signal and digitizes it by a 100 MHz flash analog-to-digital converter (FADC). The digitized signals can then be used by the fast programmable gate array (FPGA)(part of the Type 2 board), which operates according to different algorithms, programmable in a simple and flexible way [13].

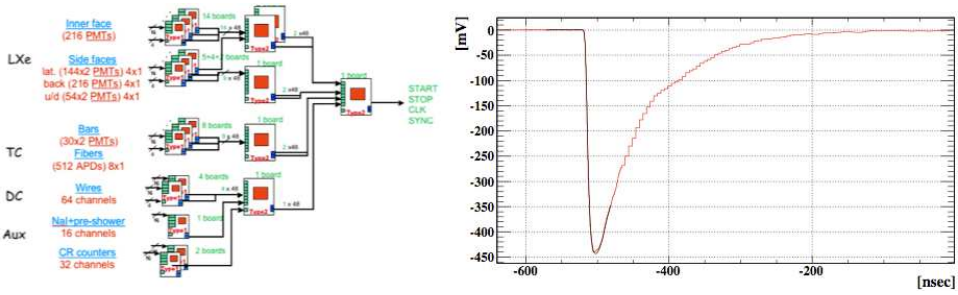

Fig. 8. The trigger tree structure (at left). A waveform as digitized by the DRS (at right).

The system allows individual corrections to each PMT signal: the different PMT gain and quantum efficiency can be taken into account and the baseline of each signal can be subtracted (the latter feature is for example essential for correctly evaluating the energy deposited in the LXe calorimeter).

3.6. The DAQ system

The signal digitization is obtained by a 2 GHz waveform which samples a CMOS chip. The waveform sampling was adopted to cope better with a possible event pile-up at the high MEG rates. The adopted solution is based on a capacitor sampling chip, previously developed at PSI.

The domino sampling chip is characterized by a sampling speed of 2 GHz (500 ps bin width; necessary to obtain a timing resolution of 50 ps), with the domino wave permanently circulating until stopped by the trigger. This new chip is called the domino ring sampler [14]. The number of storage capacitors is 1024, and the readout speed, via the shift register, is 40 MHz.

The DAQ system of the MEG experiment uses the DRS chip on all 1000 PMT channels (LXe calorimeter and TC) at a sampling speed of 2 GHz and on all 3000 drift chamber channels (chatodes and anodes) at a sampling speed of 500 MHz. A timing calibration signal is distributed and sampled in all DRS chips, meeting the requirement for a 100 ps timing accuracy.

3.7. The calibration methods

Several calibration and monitoring methods were developed to ensure that the required detector performances were reached and maintained during the measurement, guaranteeing a reliability of the physics results [15].

The energy and time resolutions of the LXe calorimeter at an energy $E_\gamma = 54.9$ MeV, close to the γ-energy from muon decay, are measured by means of the negative pion charge exchange reaction $(\mathrm{p}(\pi^-, \pi^0)\mathrm{n}$, followed by the decay $\pi^0 \to \gamma\,\gamma$. The γ at the requested energy is selected by using an auxsiliary NaI detectorr, mounted in front of the LXe calorimeter.

The rapid and frequent light-yield monitoring and the calorimeter uniformity checks are done by means of the sharp 17.6 MeV γ-line, associated with the resonant reaction ${}^{7}_{3}\mathrm{Li}(\mathrm{p},\gamma){}^{8}_{4}\mathrm{Be}$ (Fig. 9).

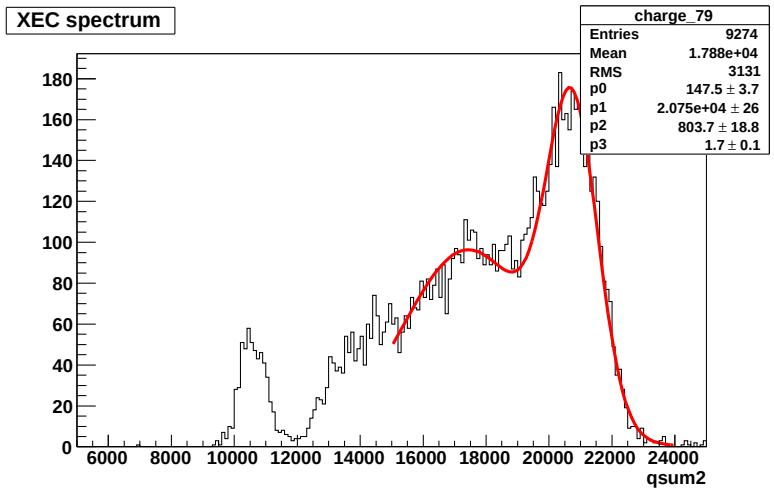

Fig. 9. The 17.6 MeV γ-line from the ${}^{7}_{3}\mathrm{Li}(\mathrm{p},\gamma){}^{8}_{4}\mathrm{Be}$ resonant reaction.

The LXe calorimeter energy scale and linearity are obtained combining the previuos γ-lines with the others, at 4.4 MeV and 11.7 MeV, which come from the ${}^{11}_{5}\mathrm{B}(\mathrm{p},\gamma){}^{12}_{6}\mathrm{C}$ reaction.

The γ's from the boron reaction are simultaneous and used to synchronize the LXe calorimeter and the timing counter (TC) (offset determination). The relative $\mathrm{e}^+ - \gamma$ timing resolution, close to the signal one, is measured by means the radiative muon decay.

The energy scale and the resolution, and the angular resolution of the spectrometer are determinated by the edge of the Michel spectrum.

4. The 2009 detector performance

Table 1 summarizes the detector performance reached during the 2009. Each variable is also compared with the 2008 measured values. The 2009 data taking period was short and the data quality is very good. In this section we present some rapresentative plots for the main kinematic variables.

Figure 10 shows liquid xenon ligth yield as a function of the time. The 17.6 MeV γ-line was used for this purpose. The expected light yield was reached after a short Xe purification in liquid phase and maintained at the level of 1% during the physics run.

The LXe energy resolution at 54.9 MeV was measured by the low-energy selected γ from the π^0 decay, as explained above. A $\sigma_E = 1.54 \pm 0.06\%$ was obtained,

TABLE 1. The MEG detector performances during the 2008 and the 2009 (Resolutions in sigma).

Variable(σ)	2008	2009
Gamma energy (%)	2.0 (depth $>$ 2.0 cm)	2.0 (depth $>$ 2.0 cm)
Gamma timing (psec)	80	$>$ 67
Gamma position (mm)	5 - 6	5 - 6
Gamma efficiency (%)	63	58
Positron momentum (%)	1.6	0.74 (core)
Positron timing (psec)	$<$ 125	$<$ 125
Positron angle (mrad)	10(ϕ)-18(θ)	7.4(ϕ)-11.2 (θ)
Positron efficiency (%)	14	40
Gamma-positorn timing (psec)	148	142 (core)
Muon decay point (mm)	3.2 (R) - 4.5 (Z)	2.3 (R) - 2.8 (Z)
Trigger efficiency (%)	66	84
DAQ time/real time (days)	48/78	35/43
Stopping muon rate (s^{-1})	3×10^7	2.9×10^7
Sensitivity	1.3×10^{-11}	6.1×10^{-12}
B.R. upper limit	2.8×10^{-11}	1.5×10^{-11}

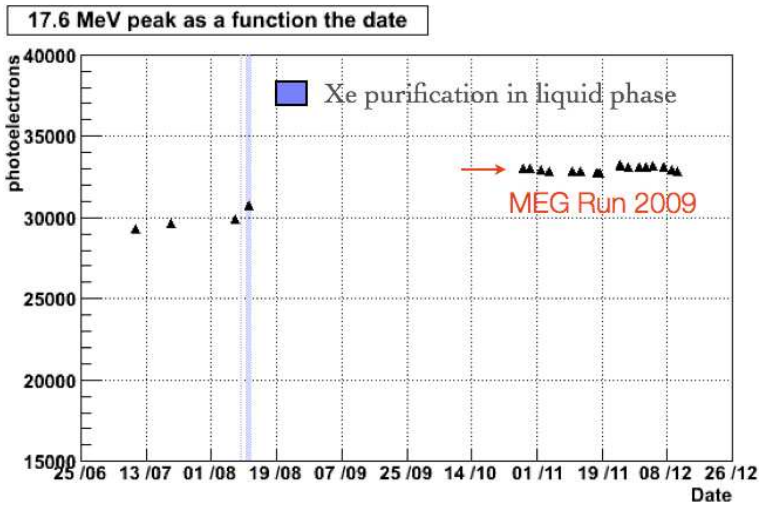

Fig. 10. Xenon light yield monitoring during 2009. The peak refers to 17.6 MeV *γ-line.*

which means $\sigma_E = 1.95$ at 52.9 MeV, the signal energy (Fig. 11). Figure 12 shows the Michel positron energy spectrum edge, on which the energy resolution of the spectrometer can be evaluated ($\sigma_E = 0.74\%$ at 52.9 MeV). Finally, Fig. 13 shows a very clean peak from the radiative muon decay. The measured LXe-timing counter timing resolution is 149 ± 10 ps, equivalent to 142 ps at the signal region (radiative γ energy: $40 \leq E_\gamma \leq 45$ MeV).

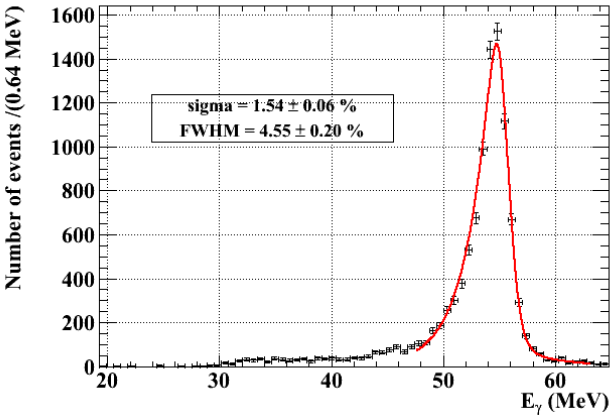

Fig. 11. Gamma spectrum for the LXe calorimeter. Events from negative pion charge exchange reaction on proton.

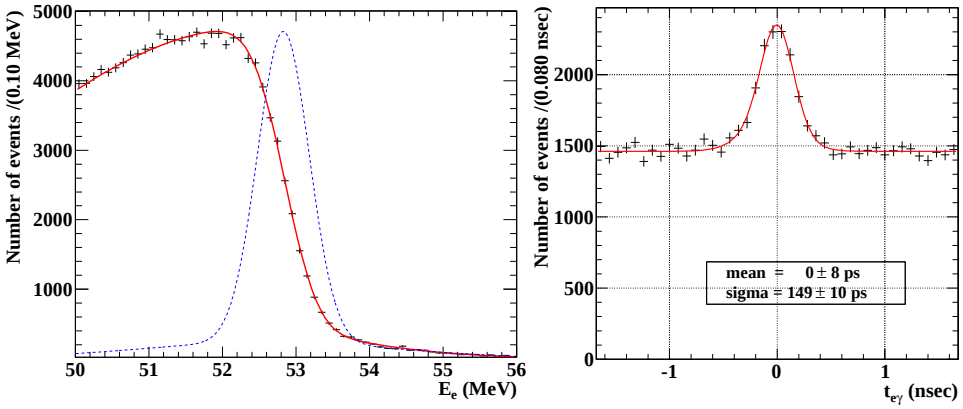

Fig. 12 (left). Positron spectrum for the DCH+COBRA spectrometer. Events from standard muon decay.

Fig. 13. The relative time distribution $t_{e\gamma}$ showing the radiative Michel decay peak during physics runs, for $40 \leq E_\gamma \leq 45$ MeV.

5. *The analysis strategies*

The physics results are based on likelihood analysis. The collected sample is saved and a preliminary data reduction is performed. These pre-selected events are further processed. The events falling into a pre-defined window ("blinding-box"), containing the signal region on the E_γ-ray and on the $t_{e\gamma}$, were saved in separate hidden files; the $\mu \to e\gamma$ decay is searched within this sample. The other events

("side-bands") are used for optimizing the analysis parameters and for studying the background.

The blinding-box is opened after completing the optimization of the analysis algorithms and the background studies.

Figure 14 shows the analysis and blinding boxes in the $(E_\gamma, t_{e\gamma})$-plane.

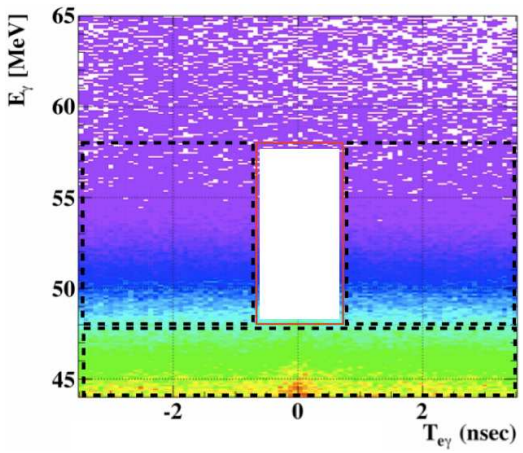

Fig. 14. Analysis and blinding boxes in the $(E_\gamma, t_{e\gamma})$-plane.

A candidate $\mu \to e\gamma$ event is characterized by the measurement of five kinematical parameters: the positron energy E_e, gamma energy E_γ, relative time between positron and gamma $t_{e\gamma}$ and the opening angles between the two particles $\theta_{e\gamma}$ and $\phi_{e\gamma}$.

A likelihood function is built in terms of the signal and the two kinds of background: the radiative Michel decay and the accidental background. A probability density function (PDF), depending on the five kinematical parameters, is associated to each component; the likelihood has the following expression

$$\mathcal{L}(N_{sig}, N_{RMD}, N_{BG}) = \frac{N^{N_{obs}} e^{-N}}{N_{obs}!} \prod_{i=1}^{N_{obs}} \left[\frac{N_{sig}}{N} S + \frac{N_{RMD}}{N} R + \frac{N_{BG}}{N} B \right]. \quad (1)$$

The signal PDF S is obtained as the product of the PDFs for the five observables (E_γ, E_e, $t_{e\gamma}$, $\theta_{e\gamma}$ and $\phi_{e\gamma}$). The radiative Michel decay PDF R is the product of the theoretical PDF (in terms of the correlated E_γ, E_e, $\theta_{e\gamma}$ and $\phi_{e\gamma}$), folded with the detector response, and the measured $t_{e\gamma}$ PDF (the same of the signal one); the PDF B is the product of the background spectra for the five observables, which are precisely measured in the data sample in the side-bands.

Figure 11 and Fig. 13 (previous section) are two examples of PDF for the γ energy and the $e - \gamma$ relative timing of the signal. Figure 15 shows γ energy background from the sideband events (green: radiative Michel decay, blue: annihilation in flight). No unexpected background is present.

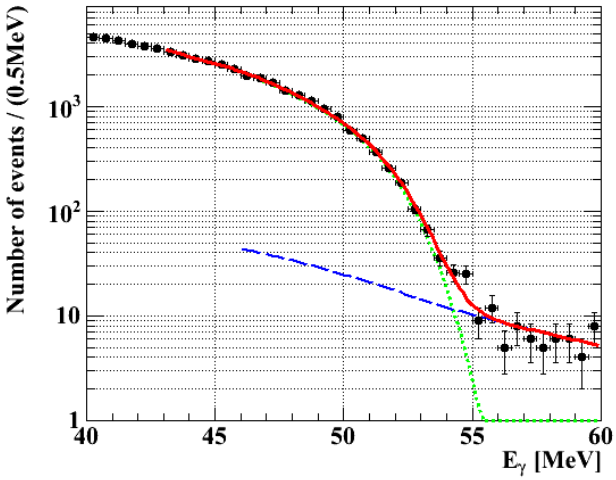

Fig. 15. Distribution of E_γ for all events in the analysis window. A solid line shows the projection of the fitted likelihood function.

6. *The 2009 data sample*

The total number of muons stopped on the target was $6.5 \cdot 10^{13}$.

The 90% confidence intervals are calculated by three indipendent likelihood fitting tools, all based on the Feldman-Cousins approach [16]. All results are consistent.

N_{sig}, N_{RMD} and N_{BG} are extracted by a likelihood fit on the observed events in the signal region. The likelihood ratio ordering technique is used to determine the BR($\mu^+ \to e^+\gamma$). To evaluate the 90% confidence interval for N_{sig}, the N_{BG} is fixed and a contour of 90% C.L. on the (N_{sig}, N_{RMD})-plane is constructed by means of toy Monte Carlo simulations.

Figure 16 show the events which are found inside the blinding box. The different blue lines correspont to 1σ, 1.64σ and 2σ. For each plot cut on the other variables are applied (for a 90% window). This event number corresponds to an upper limit on $N_{sig} \leq 14.5$, at 90% C.L. and the best fit for N_{sig} is equal to 3. The upper limit includes the sistematic uncertainties. The upper limit on BR($\mu^+ \to e^+\gamma$) was calculated by the C.L. intervals normalizing the upper limit on N_{sig} to the Michel positrons counted simultaneously with the signal, with the same analysis cuts, assuming BR($\mu^+ \to e^+\nu_e\overline{\nu}_\mu$) ≈ 1. This method has the advantage of being indipendent of the instantaneous beam rate and is nearly insensitive to the positron acceptance and efficiency factors associated with the DCH and TC, which differ only for small momentum-dependent effects between the signal and the normalization sample.

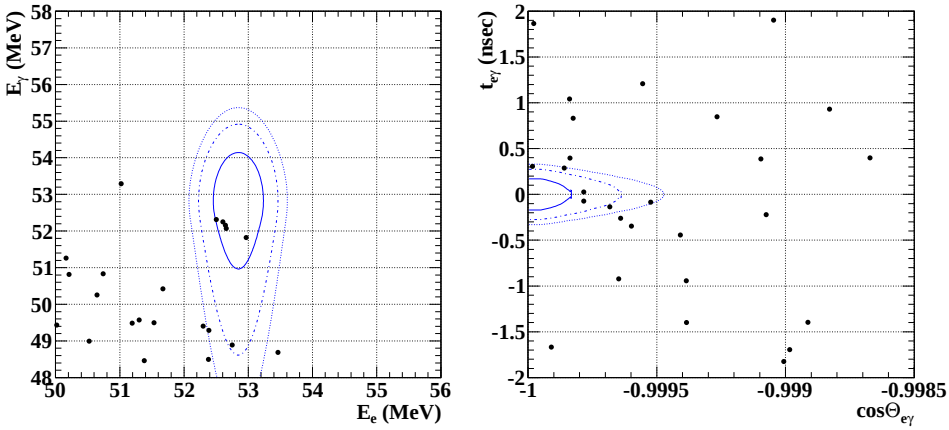

Fig. 16. Events inside the blinding box, in the (E_γ-E_e)-plane (left) and ($t_{e\gamma}$-cos$\Theta_{e\gamma}$)-plane (right).

The branching ratio can be written as

$$\mathrm{BR}(\mu^+ \to \mathrm{e}^+\gamma) = \frac{\mathrm{N_{sig}}}{\mathrm{N_{e\nu\overline{\nu}}}} \times \frac{\mathrm{f^E_{e\nu\overline{\nu}}}}{\mathrm{P}} \times \frac{\epsilon^{\mathrm{trg}}_{\mathrm{e\nu\overline{\nu}}}}{\epsilon^{\mathrm{trg}}_{\mathrm{e\gamma}}} \times \frac{\mathrm{A^{TC}_{e\nu\overline{\nu}}}}{\mathrm{A^{TC}_{e\gamma}}} \times \frac{\epsilon^{\mathrm{DCH}}_{\mathrm{e\nu\overline{\nu}}}}{\epsilon^{\mathrm{DCH}}_{\mathrm{e\gamma}}} \times \frac{1}{\mathrm{A^g_{e\gamma}}} \times \frac{1}{\epsilon_{\mathrm{e\gamma}}} \qquad (2)$$

where $N_{e\nu\overline{\nu}}$ is the number of detected Michel positrons with $50 \leq E_e \leq 56$ MeV; P is the prescale factor in the trigger used to select Michel positrons; $f^E_{e\nu\overline{\nu}}$ is the fraction of Michel positron spectrum above 50 MeV; $\epsilon^{trg}_{e\gamma}/\epsilon^{trg}_{e\nu\overline{\nu}}$ is the ratio of signal-to-Michel trigger efficiencies; $A^{TC}_{e\gamma}/A^{TC}_{e\nu\overline{\nu}}$ is the ratio of the signal-to-Michel DCH-TC matching efficiency; $\epsilon^{DCH}_{e\gamma}/\epsilon^{DCH}_{e\nu\overline{\nu}}$ is the ratio signal-to-Michel DCH recostruction efficiency and acceptance; $A^g_{e\gamma}$ is the geometrical acceptance for gamma signal given an accepted signal positron; $\epsilon_{e\gamma}$ is the efficiency of gamma recostruction and selection criteria.

The quoted limit on the branching ratio of the $\mu^+ \to e^+\gamma$ decay is therefore

$$\mathrm{BR}(\mu^+ \to \mathrm{e}^+\gamma) \leq 1.5 \times 10^{-11} \text{ (90\%C.L.)} \qquad (3)$$

where the systemetic uncertainty on the normalization is taken into account.

7. *The LFV in the other muonic channels*

The other muonic channels which violate the leptonic flavour are (a) the muon decay into three charged particles $\mu^\pm \to e^\pm e^- e^+$ and (b) the muon-to-electron conversion in a nucleus $\mu^- N \to e^- N$ [17].

The relative branching ratios of the lepton flavour violating muon decays strongly depends on the theoretical models. Looking only for the electromagnetic

gauge-invariant transition amplitudes, the BR($\mu^+ \to e^+\gamma$) is $\mathcal{O}(100)$ times larger than BR($\mu^\pm \to e^\pm e^- e^+$) or BR($\mu^- N \to e^- N$). In this theoretical scheme the $\mu^+ \to e^+\gamma$ process is favoured but the BR of the other muonic channel, i.e. the μ-to-e conversion, is greatly enhance in other scenarios. A complete knowledge of this physics section can be reached only searching for all LVF muonic channels.

The present upper limit on the $\mu^\pm \to e^\pm e^- e^+$ decay was obtained by the SINDRUM experiment in 1998, BR($\mu^+ \to e^+ e^- e^+$) $< 1.0 \times 10^{-12}$.

Positive muons were used to avoid muonic atomic formation. A continuous muon beam ($I_\mu \approx 10^6 \mu/s$) was requested to reduce the accidental background source, where three particles are present; this background was also the main one. Possible improvements could be reached by using the present muon beam intensity ($I_\mu \approx 10^8 \mu/s$) to improve the sensitivity by two orders of magnitude.

In order to be competitive with $\mu^+ \to e^+\gamma$ or $\mu^- N \to e^- N$ searches, a sensitivity down to some 10^{-16} is desiderable.

The main experimental challenge is to develop tracking devices able to work at high rates. Because the background increases linearly with the muon rate squared, background reduction must improve by more than three orders of magnitude.

The best upper limit on the $\mu^- N \to e^- N$ process was measured by the SINDRUM II experiment, by using golden nuclei: BR($\mu^- Au \to e^- Au$) $< 7 \times 10^{-13}$.

A negative muon beam was used. From the experimental point of view the main difference of this search with respect to the other ones is the event signature: a monochromatic electron. There are no accidental backgrounds: improvements can come pushing on the muon beam intensity to a very high value ($I_\mu \approx 10^{10} - 10^{11} \mu/s$). With this beam intensity, a sensitivity at the level of 10^{-16} can be reached.

Obtaining such a high muon rate, with a narrow spectrum and a low contamination, is a major challenge. Projects as Mu2e and COMET aim to develop this kind of facility to start running experiment on $\mu^- N \to e^- N$ after that the MEG experiment draws to a close.

8. The LFV in the tauonic channels

The lepton flavour violating tauonic channel number is more likely than the muonic one thanks to the large τ mass ($m_\tau \approx 1.78$ GeV ≈ 18 m$_\mu$). The possible processes are: $\tau^\pm \to l^\pm\gamma$, $\tau^\pm \to l^\pm l^+ l^-$ (from now $\tau \to 3\ l$) and $\tau^\pm \to l^\pm h^0$, where l stays for the muon or the electron and h^0 indicates a neutral hadron.

In many SUSY and SUSY-GUT schemes, the tau LFV BR are enhanced with respect to the muon LFV decay by a factor $(m_\tau/m_\mu)^\alpha$, with $\alpha \geq 3$, which means i.e. BR($\tau^\pm \to \mu^\pm\gamma$)/BR($\mu^\pm \to e^\pm\gamma$) $\approx 10^{3\,\mathrm{to}\,5}$.

The best upper limit comes from the tau decay into three charged leptons, by the BELLE and BaBar experiment (BR($\tau \to 3\ l <$ few 10^{-8})). B factories are in fact τ-factories. Sensitivity at level of $10^{-(9\,\mathrm{to}\,10)}$ is desiderable. This sensitivity

could be reached by means the new $e^+ - e^-$ collider, with higher intensity, as KEKB upgrade or SuperB facility.

Figure 17 summarizes the muonic and tauonic LFV searches [17].

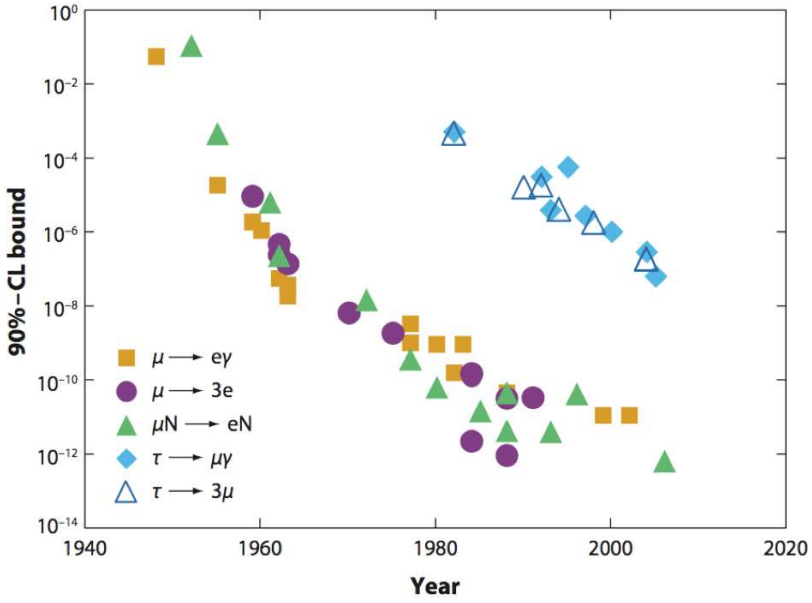

Fig. 17. Muonic and tauonic LFV searches.

9. *Conclusion*

MEG started to collect data at the end of 2008 [18]. A new data sample was acquired at the end of 2009, for a period of 1.5 months. An upper limit on BR($\mu \to e\gamma$) $< 1.5 \times 10^{-11}$ was determined. The long data taking period was started and a new result with more statistics is assumed from the 2010 data. A sensitivity at the level of a few $\times 10^{-13}$ is expected in the next three years.

References

[1] M. L. Brooks et al. (MEGA collaboration), Phys. Rev. Lett. **83** (1999) 1521.

[2] R. Barbieri and L. J. Hall, Phys. Lett. B **338** (1994) 212.

[3] R. Barbieri, L. J. Hall and A. Strumia, Nucl. Phys. B **445** (1995) 219.

[4] Y. Kuno and Y. Okada, Rev. Mod. Phys. **73** (2001) 151.

[5] M. Raidal et al., *Flavour Physics of Leptons and Dipole Moments*, arXiv:0801.1826v1.

[6] L. Calibbi et al., *Lepton Flavour Violation from SUSY-GUTs: where do we stand for MEG, PRISM/PRIME and a Super Flavour Factory*, hep-ph/0605139.

[7] A. Baldini et al., *Research Proposal to INFN* (2002).
[8] A. Badertscher et al., Nucl. Instr. Meth. A **238** (1985) 200.
[9] A. Baldini et al., Nucl. Instr. Meth. A **545** (2005) 753.
[10] A. Baldini et al., Nucl. Instr. Meth. A 566 (2006) 294.
[11] A. Baldini et al., IEEE Trans. Diel. Elec. Ins. **13** (2006) 547.
[12] M. Bonesini et al., Nucl. Instr. Meth. A **465** (2007) 753.
[13] L. Galli, IEEE NSS-MIC-RTSD, Dresden, Germany (2008) N30-468, 2625.
[14] S. Ritt, Nucl. Instr. Meth. A **494** (2002) 520.
[15] A. Papa, Il Nuovo Cimento B **122** (2007) 627.
[16] G. J. Feldman and R. D. Cousins, Phys. Rev. D **57** (1998) 3873.
[17] W. J. Marciano, T. Mori and J. M. Roney, Ann. Rev. Nucl. Part. Sci. **58** (2008) 315.
[18] J. Adam et al. (MEG Collaboration), Nucl. Phys. B **834** (2010) 1.

NOVI ISHODI MJERENJA MEG ZA $\mu^+ \to e^+\gamma$ RASPAD

Cilj eksperimenta MEG je određivanje omjera grananja za rijetki muonski raspad $\mathrm{BR} = \dfrac{\mu^+ \to \mathrm{e}^+\gamma}{\mu^+ \to \mathrm{e}^+\nu_\mathrm{e}\overline{\nu}_\mu}$ na razini od $\approx 10^{-13}$. Da bi se taj cilj postigao, u mjerenju se rabe najintenzivniji postojeći muonski snopovi ($\approx 10^8\mu$/s) i moraju se postići najviša moguća razlučivanja energije, vremena i položaja. MEG je započeo sakupljanje podataka krajem 2008. Tijekom 2009 je velik dio mjerenja bio posveén baždarenjima i optimizaciji rada detektora; tijekom mjesec i po dana krajem 2009. godine sakupljen je i nov niz mjernih podataka. Opisujemo osnovna svojstva svakog detektorskog dijela i mjerenih razlučivanja, te predstavljamo ishode traganja za $\mu^+ \to e^+\gamma$ raspadom na osnovi uzorka podataka iz 2009.